www.advintellsyst.com

Multiple Sampling Capsule Robot for Studying Gut Microbiome

Sanghyeon Park, Manh Cuong Hoang, Jayoung Kim, and Sukho Park*

Longitudinal analysis of the gut microbiota is crucial for understanding its relationship with gastrointestinal (GI) diseases and advancing diagnostics and treatments. Most ingestible sampling devices move passively within the GI tract, rely on physiological factors, and fail at multipoint sampling. This study proposes a multiple-sampling capsule robot capable of collecting gut microbiota from various locations within the GI tract with minimal cross-contamination. The proposed capsule comprises a body, a driving unit, six sampling tools, a central rod, and two heads. Electromagnetic field control facilitates control of the orientation and position of the capsule, particularly to align the channel of the capsule where the sample is collected facing downward. The capsule can collect six gut microbiota samples preventing contamination before and after sampling. The active locomotion and multiple sampling performance of the capsule are evaluated through basic performance tests (propulsion direction precision: $0.76 \pm 0.52^{\circ}$, channel alignment precision: $0.84 \pm 0.55^{\circ}$), phantom tests (average amount per sample: 10.3 \pm 2.4 mg, cross-contamination: 0.6 \pm 0.4%), and ex-vivo tests (average amount per sample: 9.9 \pm 1.7 mg). The possibility of integration and clinical application of the capsule is confirmed through preclinical tests using a porcine model.

S. Park, S. Park

Department of Robotics and Mechatronics Engineering Daegu Gyeongbuk Institute of Science and Technology (DGIST)

Daegu 42988, South Korea E-mail: shpark12@dgist.ac.kr

L-mail. silparkiz@ugist.ac

M. C. Hoang

School of Electrical and Electronics Engineering Hanoi University of Science and Technology (HUST)

Hanoi 100000, Vietnam

J. Kim

Korea Institute of Medical Microrobotics (KIMIRo) Gwangju 61011, South Korea

J. Kin

Department of Biosystems Engineering Chungbuk National University Cheongju 28644, South Korea

The ORCID identification number(s) for the author(s) of this article can be found under https://doi.org/10.1002/aisy.202300625.

© 2024 The Author(s). Advanced Intelligent Systems published by Wiley-VCH GmbH. This is an open access article under the terms of the Creative Commons Attribution License, which permits use, distribution and reproduction in any medium, provided the original work is properly cited.

DOI: 10.1002/aisy.202300625

1. Introduction

Gut microbiota is a diverse microbial community in the digestive tract, encompassing bacteria, archaea, viruses, and fungi. Emerging research findings have emphasized the significant roles of gut microbiota in human health and disease. Consequently, related studies have garnered increased attention in recent years. The importance of gut microbiota research can be elucidated as follows. First, the gut microbiota is crucial for maintaining intestinal health. They assist in breaking down ingested foods and extracting nutrients, modulating the immune system, and protecting against harmful pathogens.[1-4] Second, an imbalance in the gut microbiota, termed dysbiosis, is closely associated with a wide range of diseases, including inflammatory bowel disease (IBD), obesity, diabetes, autoimmune diseases, and cancer. [5-15] Third, recent findings have suggested that the gut microbiota can potentially influence mental health and cognitive functions. For

instance, changes in the gut microbiota can affect mood, anxiety, depression, autism, and Alzheimer's disease. [16–20] Finally, the gut microbiota is significantly influenced by factors related to diet and lifestyle, such as the type of food consumed, levels of physical activity, and exposure to antibiotics and other medications. Therefore, the impact of these factors on the gut microbiota must be understood to facilitate the promotion of healthy dietary and lifestyle choices and reduce the risk of diseases. [21–24]

Longitudinal analysis and biogeography of gut microbiota have become indispensable for the diagnosis and treatment of gastrointestinal (GI) diseases. Lavelle et al. investigated the spatial variation of colonic microbiota in patients with ulcerative colitis and control volunteers. They found that the composition of colonic microbiota in patients varied depending on their location. [25] Dahl et al. reported that the therapeutic effects of mesalamine, which is commonly used for IBD treatment, could be influenced by the gut microbiota. [26] However, mesalamine is less effective in treating IBD in the upper GI tract than in the lower GI tract. These findings highlight the importance of examining the gut microbiota at multiple time points to improve the diagnosis, prognosis, and treatment of GI diseases. If the gut microbiota throughout the entire GI tract in a single individual could be studied, the dynamics of the gut microbiota, its relevance to various GI diseases, and the factors that influence its composition and function could be understood. Ultimately,

www.advancedsciencenews.com www.advintellsyst.com

research on the longitudinal analysis and biogeography of gut microbiota is expected to offer numerous opportunities to enhance the quality of life of patients with GI diseases.^[27]

Stool analysis is a non-invasive method commonly used in gut microbiota research owing to the ease of collection. However, analysis of the gut microbiota using stool samples has a limitation. The gut microbiota is unevenly distributed throughout the GI tract, and the microbial composition varies depending on its location; [28,29] thus, fecal microbiota primarily reflects the luminal microbiota of the colon, with minimal representation of the microbiota in the small intestine. [25,30,31] To address this, invasive sampling methods involving endoscopy such as biopsy, luminal brushing, and catheter aspiration have been employed. These methods can provide valuable insights into gut microbiome analysis spanning the entire GI tract. [32-36] However, endoscopy-based gut microbiota sampling requires sedation or anesthesia, can be uncomfortable for the patient, and carries the risk of complications, such as bleeding or perforation. Moreover, this method facilitates sampling only from specific areas of the GI tract, and accessing hard-to-reach areas such as the distal small intestine and proximal colon, is challenging. Furthermore, this method can result in changes in the gut microbiota during bowel preparation.[37]

Recently, various ingestible sampling devices have been proposed to address the limitations of existing sampling methods. Shalon et al. introduced a sampling capsule capable of measuring gut microbiome and bile acid profiles under physiological conditions.[38] The capsule comprises a vacuum-collection bladder and a dissolvable body. Four capsules have been reported, each designed to collect gut microbiota at specific locations: the proximal small intestine, mid-small intestine, distal small intestine, and proximal colon. Nejati et al. proposed a smart capsule to sample the proximal colonic microbiome. [39] The design features a pH-sensitive double layer, hydrogel block, polydimethylsiloxane (PDMS) lid, and chamber. The first layer prevents sampling in the stomach and dissolves in the small intestine, whereas the second prevents sampling in the small intestine and dissolves in the colon. Once both layers are dissolved, the intestinal fluid containing the gut microbiota is drawn into the chamber through the entrance of the capsule, causing the hydrogel block to expand. This action prompts the PDMS lid above the hydrogel block to seal the entrance and prevent cross-contamination. However, such capsules can initiate microbial sampling actions based on the intestinal pH environment, and cannot perform selective or multiple samplings. [40,41] Rehan et al. developed a robotic capsule for in vivo gut microbiome sampling. [42] The capsule comprised a chamber, sampler, shape memory alloy (SMA) spring actuator, electronic board, and battery. Upon the application of a current to the SMA, the sampler is deployed by heating and stored through natural cooling. This achieves sample collection, storage, and contamination prevention. Shokrollahi et al. developed a magnetically actuated capsule to realize minimally invasive sampling of the GI microbiome. [43] The capsule comprises a body and two permanent magnets; the body incorporates a hinge and a chamber and is made of a soft elastomer. When exposed to a strong external magnetic field, the capsule opens to allow microbial sampling. Following collection, the attraction between the two internal permanent magnets causes the capsule to close, thereby preventing contamination of the collected samples. However,

Adv. Intell. Syst. 2024, 7, 2300625

capsules that mechanically collect gut microbiota have potential risks, such as causing intestinal injury during activation of the mechanism. Moreover, multiple sampling cannot be performed at various locations.[44]

This study proposed a multiple-sampling capsule robot (MSCR) capable of collecting gut microbiota from multiple locations within the GI tract while minimizing cross-contamination. Figure 1a illustrates the overall design of the MSCR and its components. Figure 1c,d depict the sampling tool and driving unit configurations, respectively. The proposed capsule comprised a capsule body, a driving unit, six sampling tools, a central rod, and two capsule heads. The capsule body had six channels and was characterized by groove patterns on its inner side. These grooves facilitated a 60° rotational movement of the driving unit during its reciprocating motion. The driving unit comprised a permanent magnet assembly for magnetic actuation, two pins to travel along the grooves on the inner side of the capsule body, and a soft magnetic rod designed to push and pull the sampling tools. Six sampling tools were designed to seal the channel entrances before and after sampling and to facilitate sample collection and storage. The central rod guided and constrained the movement and rotation of the driving unit along the central axis of the capsule. Finally, the upper capsule head was hemispherical in shape to reduce the effects of viscous friction within the intestine during capsule movement. The lower capsule head featured six holes to attach and deploy the sampling tools, which were connected to the six channels of the capsule body. The proposed capsule was equipped with a permanent magnet assembly in its driving unit, which allowed posture and position control of the capsule. Notably, the channel could be aligned by performing the microbiome sampling downwards. Furthermore, the multiplesampling mechanism of the capsule facilitated up to six sequential samplings, and the cross-contamination prevention structure of the sampling tool ensured that cross-contamination of the tool and channel was avoided before and after sampling. The key functionalities of the proposed MSCR were validated using basic performance, phantom, and ex-vivo tests. Finally, the feasibility of MSCR for clinical applications was confirmed through in vivo tests.

2. Overall Concept of Proposed MSCR

2.1. Design of MSCR

To develop an ingestible sampling device capable of multiple samplings of the gut microbiome within the GI tract, the following design requirements were defined. First, the capsule must be sufficiently small to smoothly pass through the pylorus and ileocecal valve within the digestive tract. Second, the capsule must facilitate posture and location control within the GI tract and the collection of gut microbiota from multiple locations. Third, the capsules must prevent cross-contamination of the collected samples. Finally, the capsule should have a simple structure and be easily operable, and the sampling process should cause minimal discomfort to subjects. [37] The proposed MSCR was developed to satisfy the design requirements. Figure 1b depicts the fully assembled MSCR and its components. Specifically, the capsule measured 11 and 26 mm in diameter and length, respectively,

and-conditions) on Wiley Online Library for rules of use; OA articles are governed by the applicable Creative Commons

ADVANCED INTELLIGENT SYSTEMS

www.advancedsciencenews.com www.advintellsyst.com

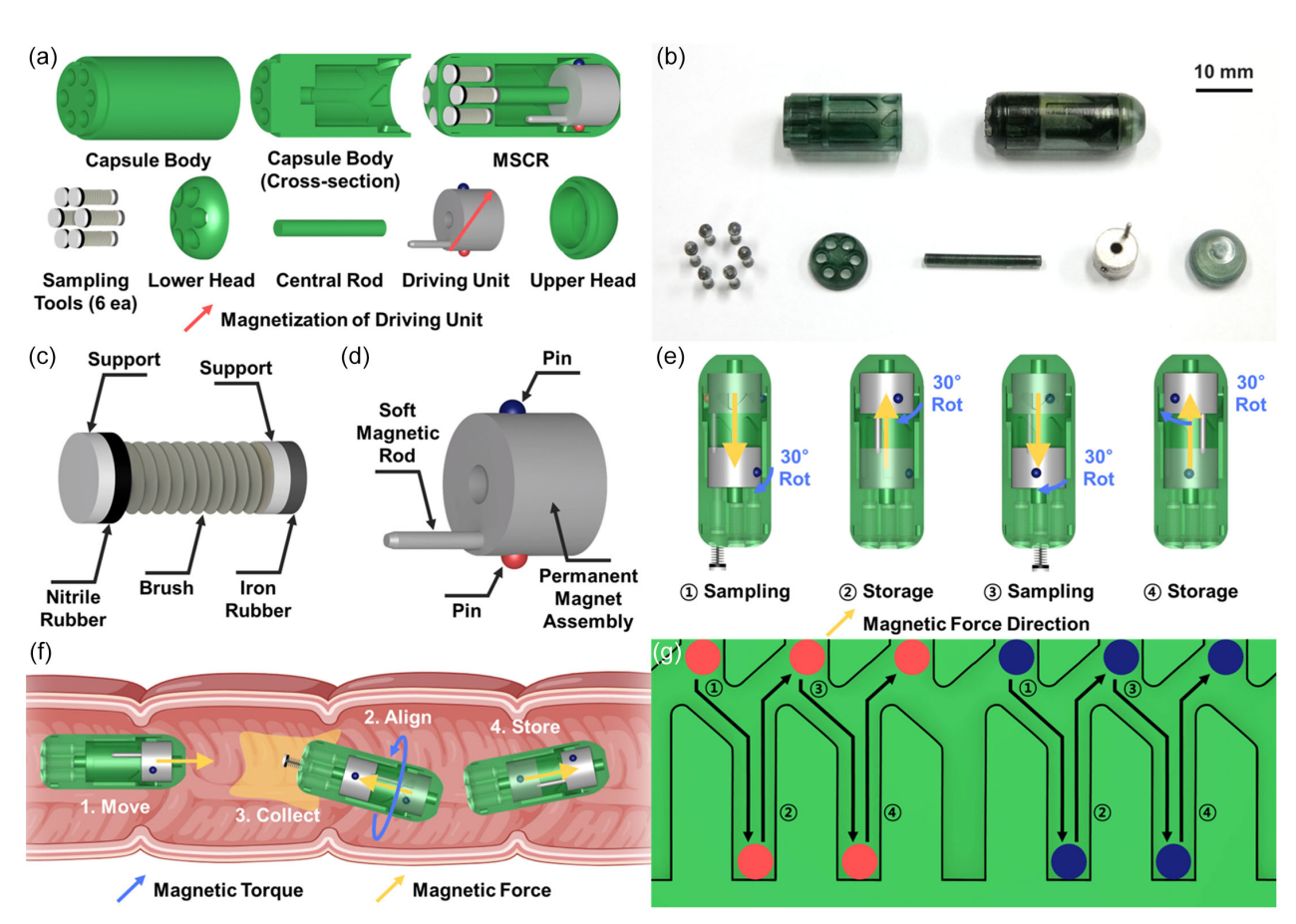


Figure 1. a) Overall design of the MSCR and its components. b) Fabricated components and fully assembled MSCR. c,d) Schematic designs of the sampling tool and driving unit. e) Working principle of the multiple-sampling mechanism. f) Sampling process. g) Open view of the inside of the capsule body. It shows the internal groove structure and depicts the path that the two pins follow during the reciprocating motion of the driving unit in the multiple-sampling process.

ensuring that it could smoothly pass through the pylorus and ileocecal valve. The capsule possessed a relatively simple multiple-sampling mechanism wherein it could actively move and adjust its posture through external magnetic fields. This facilitated multiple gut microbiome samplings. The sampling tool also exhibited a cross-contamination prevention structure, effectively preventing the contamination of the sampling tool and channel from the sampled microbiome in other sampling tools, channels, and external intestinal fluids. Consequently, the proposed MSCR method could collect microbiome samples from various locations in the GI tract, thereby minimizing cross-contamination.

Figure 1e shows the multiple-sampling mechanism of the MSCR and depicts the state of the driving unit within the capsule body during the multiple-sampling process. Figure 1g shows an open view of the interior of the capsule body, revealing the structure of the internal grooves and depicting the path followed by the two pins as the driving unit reciprocates during the multiple-sampling process. Video S1, Supporting Information, shows a digital mockup created to explain and validate the MSCR operation. It demonstrates the six-time multiple sampling process. As shown in Figure 1e,g, the structure of the driving unit included a permanent magnet assembly that facilitated the control of the

posture and position of the capsule via a magnetic field and a magnetic field gradient. The driving unit could move up and down within the capsule body along the central rod. A soft magnetic rod and two pins were attached to the top and side surfaces of the permanent magnet assembly, respectively. Here, the soft magnetic rod deploys and retrieves the sampling tool within the channel as the driving unit reciprocates. The two pins guide the driving unit as they move along the grooves on the inner side of the capsule. Specifically, when the driving unit moves from the upper to the lower head of the capsule, the soft magnetic rod aligns and inserts into one of the channels inside the capsule body, thereby pushing the sampling tool out of the channel and deploying the sampling tool out of the lower head of the capsule. This sampling tool collects the gut microbiome and fluids on the intestinal surface. Subsequently, when the driving unit moves toward the upper head of the capsule, the attraction between the iron rubber of the sampling tool and the soft magnetic rod results in the sampling tool moving with the driving unit, pulling it back into the channel for storage. By repeating this process, the proposed MSCR can perform microbiome sampling from the intestine for up to six times. Before and after performing each sampling, the rubber at both ends of the sampling tool sealed the channel entrance and exit, preventing undesirable

ADVANCED INTELLIGENT SYSTEMS

www.advancedsciencenews.com www.advintellsyst.com

cross-contamination from other sampled microbiomes and the capsule exterior.

Figure 1f illustrates the process of MSCR collection from the gut microbiome samples. First, the capsule is moved to the desired location by magnetic actuation. Initially, a magnetic field aligns the upper head of the capsule along the desired direction; subsequently, a magnetic field gradient propels the capsule along the aligned direction. This method facilitates precise capsule locomotion at the desired location within the GI tract using external magnetic field control. Second, upon reaching the target site, a magnetic field is applied to rotate the capsule such that the channel from which the sampling tool is deployed faces the GI lining. Third, a magnetic field and a magnetic field gradient are applied to propel the driving unit toward the lower head of the capsule, thereby pushing and deploying the sampling tool toward the GI lining. Fourth, the deployed sampling tool collects microbiome samples from the intestinal fluid through appropriate orientation and positioning control of the capsule. Finally, a magnetic field and a magnetic field gradient are applied to propel the driving unit toward the upper head of the capsule, pulling and storing the sampling tool within the capsule channel. By repeating these processes, the capsule can perform multiple samplings of the gut microbiome at various locations within the GI tract. After completing the multiple samplings using the proposed capsule, the capsule will be naturally excreted and retrieved, and the microbiome samples in each channel will be extracted using a micropipette. Thus, the extracted samples are analyzed by next-generation sequencing, which facilitates the identification of the microbial composition at the sampling sites.

2.2. Fundamentals of Electromagnetic Actuation Methods

Within the magnetic field, the magnetic force (F) and magnetic torque (T) applied to the permanent magnet assembly in the driving unit of the MSCR are expressed as follows:

$$\begin{pmatrix} T \\ F \end{pmatrix} = \begin{pmatrix} VM \times B \\ V(M \cdot \nabla)B \end{pmatrix} \tag{1}$$

where V and M are the volume and magnetization of the permanent magnet assembly, respectively, and B is the magnetic field flux density generated by the electromagnetic actuation (EMA) system. The magnetic field at a given position P(x, y, z) in the region of interest (ROI) can be expressed as a linear combination of the magnetic fields produced by each electromagnet in the EMA system.

$$B(P) = B_1 + B_2 + \cdots + B_n$$

$$= \begin{bmatrix} b_{x,1}(P) & \cdots & b_{x,n}(P) \\ b_{y,1}(P) & \cdots & b_{y,n}(P) \\ b_{z,1}(P) & \cdots & b_{z,n}(P) \end{bmatrix} \begin{bmatrix} i_1 \\ \vdots \\ i_n \end{bmatrix} = b(P)I$$

$$(2)$$

where B_n is the magnetic field produced by the nth electromagnet, $b(P) \in R^{3 \times n}$ is the mapping matrix, and I represents the current input vector applied to the electromagnets. The generated magnetic field was determined by multiplying the mapping matrix by the current input vector. Using Equation (1) and (2),

the magnetic field and force applied to the permanent magnet assembly can be derived as follows:

$$\begin{pmatrix} B \\ F \end{pmatrix} = \begin{pmatrix} b(P) \\ V(M \cdot \nabla)b(P) \end{pmatrix} I = X(P)I$$
(3)

where $X(P) \in \mathbb{R}^{6 \times n}$ is called as the actuation matrix. By multiplying X(P) by the current input vector for the electromagnets, both the magnetic field and force can be determined. Once the desired magnetic field and force are specified by the operator, the current input vector can be derived as follows:

$$I = \begin{pmatrix} b(P) \\ V(\mathbf{M} \cdot \nabla)b(P) \end{pmatrix}^{+} \begin{pmatrix} B_{\text{desired}} \\ F_{\text{desired}} \end{pmatrix} = X(P)^{+} \begin{pmatrix} B_{\text{desired}} \\ F_{\text{desired}} \end{pmatrix}$$
(4)

where superscript (+) denotes the pseudoinverse. Thus, the current applied to each electromagnet can be determined by multiplying the pseudoinverse matrix of X(P) by the vector comprising the desired magnetic field and desired magnetic force.

2.3. Basic Motions of MSCR

To execute multiple sampling, we defined the following four basic motions of the capsule such as capsule propulsion, channel alignment, sample collection, and sample storage. Figure 2c-f illustrates the state of the capsule and the driving unit on an arbitrary plane for each basic motion, depicting the magnetization of the driving unit, the desired magnetic field, and the desired magnetic force. Here, x' can be obtained by rotating x around z by a, and d can be obtained by rotating x' around y' by β . The desired magnetic field ($B_{desired}$) and force ($F_{desired}$) corresponding to each action of the capsule are defined as follows:

First, the $B_{desired}$ and $F_{desired}$ acting during the capsule propulsion are as follows:

$$\boldsymbol{B}_{desired} = \frac{B}{\sqrt{1 + \tan^2(\theta)}} \begin{bmatrix} c\alpha c\beta + c\alpha s\beta t\theta \\ s\alpha c\beta + s\alpha s\beta t\theta \\ s\beta - c\beta t\theta \end{bmatrix}, \ \boldsymbol{F}_{desired} = \boldsymbol{F} \begin{bmatrix} c\alpha c\beta \\ s\alpha c\beta \\ s\beta \end{bmatrix}$$
(5)

where c(*), s(*), and t(*) denote $\cos(*)$, $\sin(*)$, and $\tan(*)$, respectively. B represents the magnitude of $B_{desired}$ and F represents the magnitude of $F_{desired}$. θ is the magnetization angle of the driving unit, which is the angle between d and $B_{desired}$ and is the value of 11.1°. In practical application, only $B_{desired}$ is applied to align the upper head direction of the capsule to the desired direction, and subsequently, both $B_{desired}$ and $F_{desired}$ are applied simultaneously to propel the capsule in that direction. Here, the magnetic force should be sufficiently larger than the friction between the capsule and the intestinal surface. Since the capsule always moves in the direction its head is facing, accidental opening of the chamber can be prevented when the capsule is propelled by the magnetic field gradient.

Second, the $B_{desired}$ and $F_{desired}$ acting during the channel alignment are as follows:

$$\mathbf{B}_{\text{desired}} = \frac{B}{\sqrt{1 + \tan^2(\theta)}} \begin{bmatrix} c\alpha c\beta - c\alpha s\beta t\theta \\ s\alpha c\beta - s\alpha s\beta t\theta \\ s\beta + c\beta t\theta \end{bmatrix}, \ \mathbf{F}_{\text{desired}} = 0 \tag{6}$$

26404567, 2025, 11, Downloaded from https

brary.wiley.com/doi/10.1002/aisy.202300625 by Daegu Gyeongbuk Institute Of, Wiley Online Library on [27/11/2025]. See the Terms

conditions) on Wiley Online Library for rules of use; OA articles are governed by the applicable Creative Commons

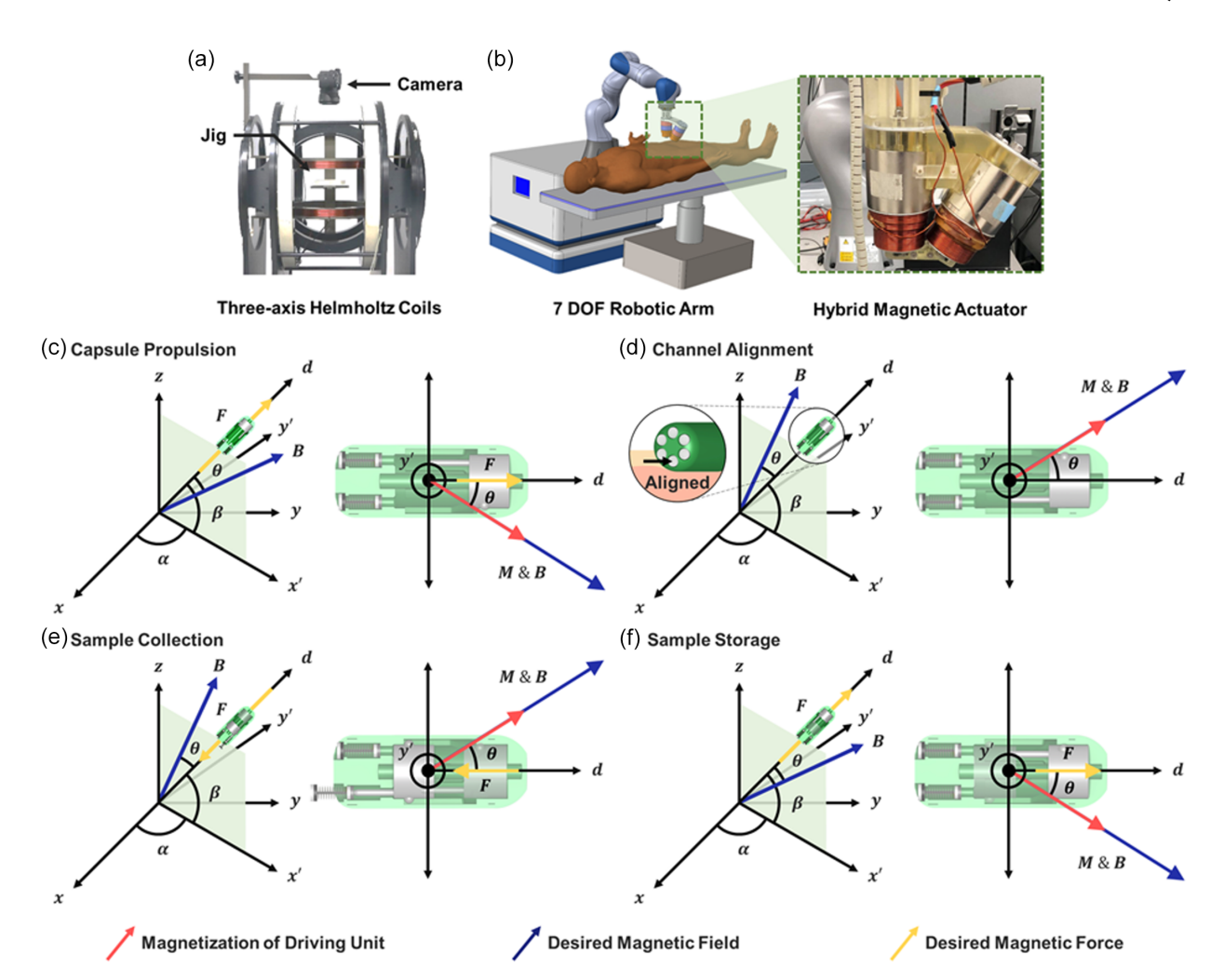


Figure 2. a) Experimental setup 1: electromagnetic coil system. b) Experimental setup 2: movable external electromagnet system. Basic motions of MSCR: c) Capsule propulsion. d) Channel alignment. e) Sample collection. f) Sample storage.

When aligning the channel of the capsule, $B_{desired}$ is applied to rotate the channel in the axial direction and align the channel through which the sampling tool will be deployed toward the GI bottom surface. Here, the strength of the magnetic field should be also sufficiently large to overcome the friction between the capsule and the intestinal surface.

Third, the $B_{desired}$ and $F_{desired}$ acting during the sample collection are as follows:

$$\mathbf{B}_{desired} = \frac{B}{\sqrt{1 + \tan^2(\theta)}} \begin{bmatrix} c\alpha c\beta - c\alpha s\beta t\theta \\ s\alpha c\beta - s\alpha s\beta t\theta \\ s\beta + c\beta t\theta \end{bmatrix}, \ \mathbf{F}_{desired} = -F \begin{bmatrix} c\alpha c\beta \\ s\alpha c\beta \\ s\beta \end{bmatrix}$$
(7)

For deploying the sampling tool, a magnetic force is applied toward the lower head of the capsule. Since the friction between the capsule body and the driving unit is less than the friction between the capsule and the intestinal surface, the driving unit can move within the capsule body. When the driving unit receives force directed toward the lower head of the capsule, it moves in this direction, causing the driving unit to rotate counter

clockwise by 30° in the capsule body. Furthermore, the pitch and yaw motions of the capsule ensure an adequate collection of microbiome sample from the intestines by the sampling tool.

Lastly, the $B_{desired}$ and $F_{desired}$ acting during the sample storage are as follows:

$$\mathbf{B}_{desired} = \frac{B}{\sqrt{1 + \tan^2(\theta)}} \begin{bmatrix} c\alpha c\beta + c\alpha s\beta t\theta \\ s\alpha c\beta + s\alpha s\beta t\theta \\ s\beta - c\beta t\theta \end{bmatrix}, \ \mathbf{F}_{desired} = \mathbf{F} \begin{bmatrix} c\alpha c\beta \\ s\alpha c\beta \\ s\beta \end{bmatrix}$$
(8)

For storing the sampling tool, a magnetic force is applied toward the upper head of the capsule. Like the deployment process, the driving unit moves within the capsule body. The distinction in the storage process is that to facilitate more accessible storage, the channel from which the tool was deployed is aligned to face the GI upper side. When the driving unit receives force toward the upper head of the capsule, the driving unit moves in this direction, causing the driving unit to rotate counter clockwise by 30° in the capsule body. Consequently, as previously described through the deployment and storage processes of the sampling tool, the driving unit moves reciprocally both

conditions) on Wiley Online Library for rules of use; OA articles are governed by the applicable Creative Commons License

ADVANCED Intelligent Systems

www.advancedsciencenews.com www.advintellsyst.com

forward and backward toward the direction of the lower head of the capsule. As illustrated in Figure 1e–g, due to the grooves within the capsule body and the two pins on the driving unit, the driving unit rotates 60° for one cycle counter-clockwise within the capsule.

3. Experimental Results

3.1. Basic Performance Tests

The fundamental performance of the MSCR was evaluated in three experiments. First, an experiment was conducted to align and propel the capsule in the desired direction. Figure 3a presents the results of the capsule propulsion experiment, showing the capsule after propulsion in all eight directions. Figure 3b depicts the propulsion angle error for each direction. The average error of the propulsion direction angle was $\approx 0.76 \pm 0.52^{\circ}$ (n = 40), which confirmed the capability of the capsule to propel along the desired direction precisely. Second, an experiment was conducted to rotate the capsule along its roll direction to align it such that the desired channel faced downward. Figure 3c presents the results of the capsule channel alignment experiment and shows the angular error of the channel alignment. The average angular error for the channel alignment was $\approx 0.84 \pm 0.55^{\circ}$ (n = 30), verifying the ability of the capsule to align the desired channel downward precisely. Compared to the results of previously reported magnetically actuated capsules the proposed capsule exhibits improved accuracy in both capsule propulsion and channel alignment. Third, an experiment was conducted to deploy and store the six sampling tools inside the capsule. Figure 3d shows the results of the deployment and storage of the tools from all six channels inside the capsule. The experiments confirmed that the capsule was successfully deployed and stored in the sampling tools without any errors.

3.2. Phantom Tests

Two phantom tests were conducted to validate the locomotion and multiple-sampling performance of the MSCR. First, an experiment was conducted using MSCR to sample three colored solutions (yellow, red, and blue) placed on the phantom. Two samples were considered for each color, resulting in a total of six samples. **Figure 4**a and Video S2, Supporting Information, depict the entire experimental process of Phantom Test 1. Figure 4a shows the final sample images retrieved from each channel of the capsule. The average amount of the sampled solution was $\approx 9.7 \pm 2.4$ mg (n = 6). Thus, MSCR could move to the desired location on the phantom, align the desired channel downwards in each target area, deploy the sampling tool, collect the colored solution, and store it inside the channel. This procedure was repeated to verify the ability of the MSCR to move on the phantom and perform multiple samplings twice for each

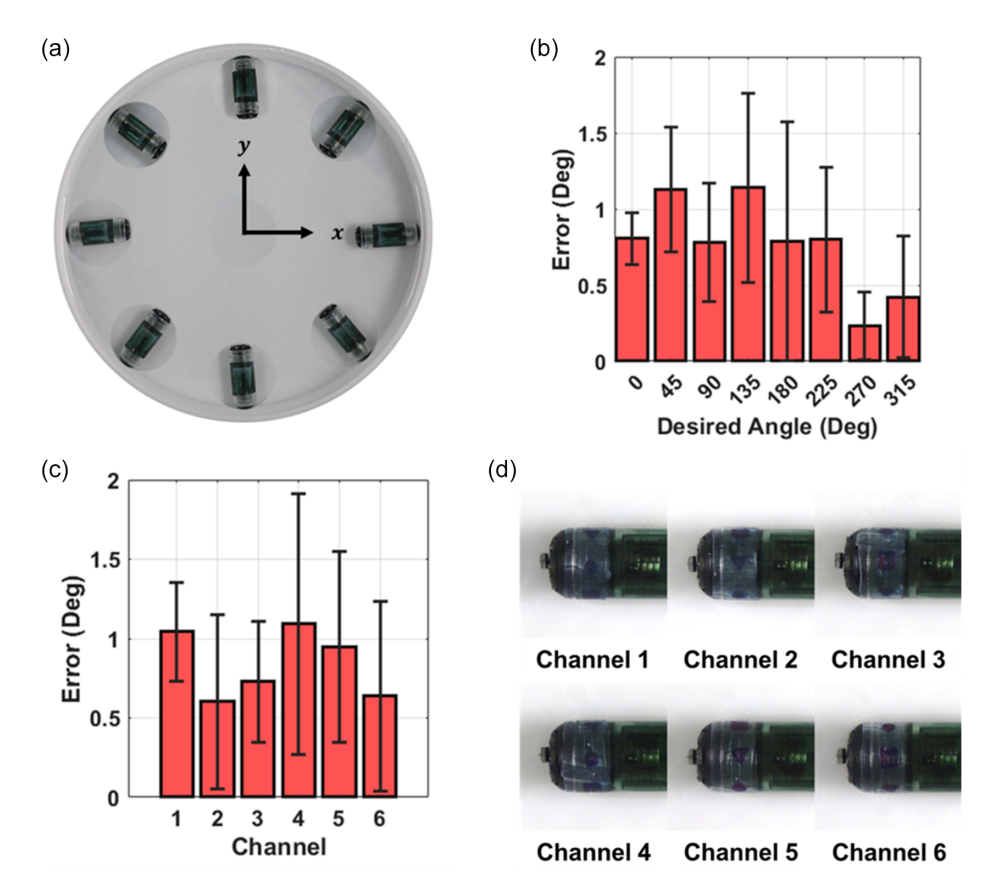


Figure 3. Basic performance tests results. a) Overlapped images of the capsule after propulsion in all eight directions. b) Propulsion direction errors. c) Channel alignment errors. d) Capsule images after deployment of the sampling tools from each channel.

26404567, 2025, 11, Downloaded from https://adv

anced.onlinelibrary.wiley.com/doi/10.1002/aisy.202300625 by Daegu Gyeongbuk Institute Of, Wiley Online Library on [27/11/2025]. See the Terms and Conditions

conditions) on Wiley Online Library for rules of use; OA articles are governed by the applicable Creative Commons

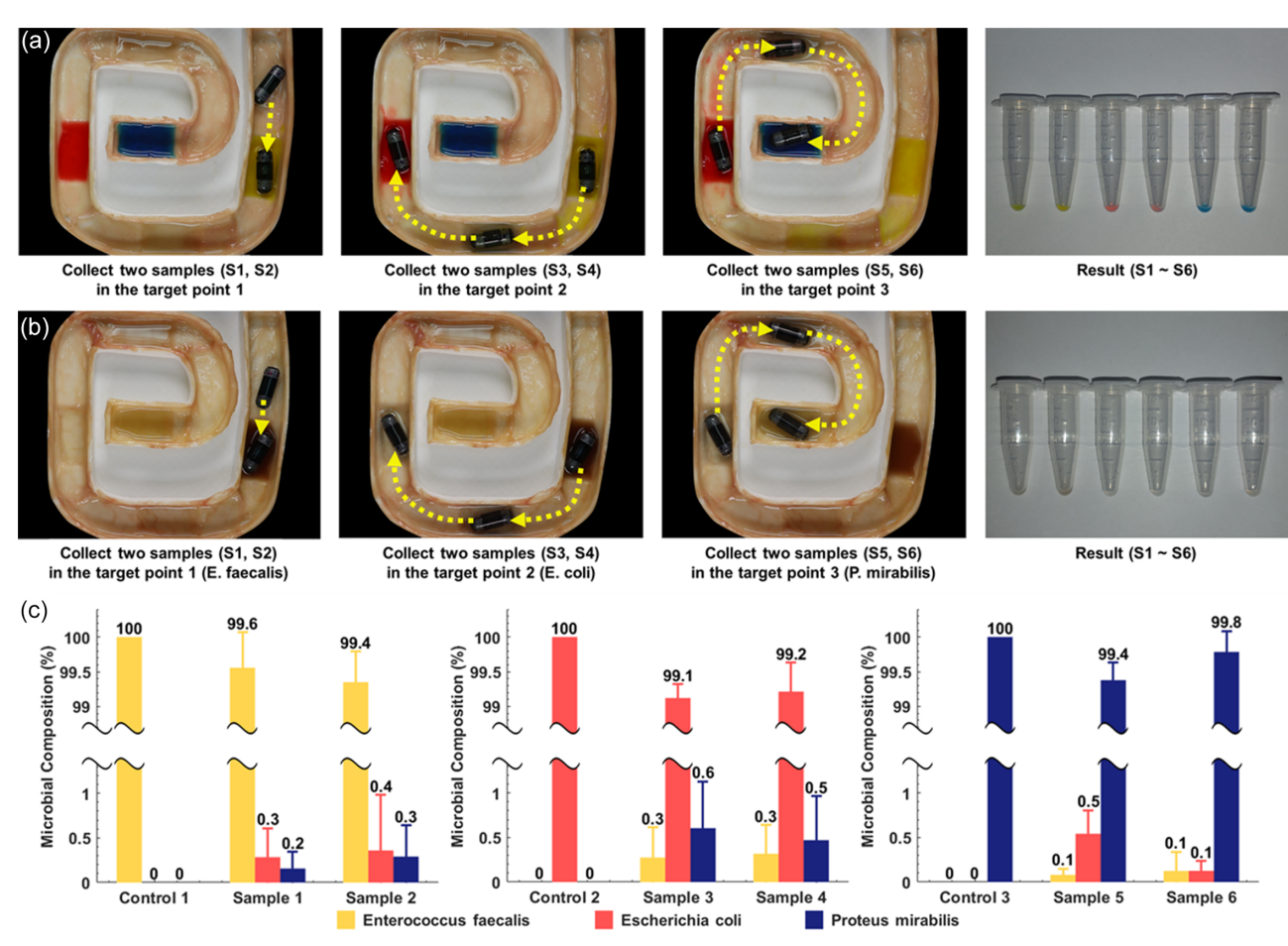


Figure 4. Phantom test results: a) Locomotion and multiple samplings of three colored PEG solutions, b) Locomotion and multiple samplings of three microbial culture liquids, and c) Microbial compositions on the color detection agar where the samples (diluted 1000 times) were cultured.

color, for a total of six samples. Furthermore, the degree of contamination between the samples collected by MSCR was minimized, ensuring that the color of each target sample remained nearly identical.

Second, an experiment was conducted using MSCR to sample three types of microbial culture solutions placed on the phantom. Two samples were considered for each type, resulting in six samples. Figure 4b and Video S3, Supporting Information, depict the entire experimental process of Phantom Test 2. Figure 4b presents the final sample images extracted from each capsule channel. The average amount of the sample was $\approx 10.3 \pm 2.4$ mg (n = 18). Similar to Phantom Test 1, the ability of the MSCR to move across the phantom and sample each microbial solution twice, for a total of six samples, was confirmed. Figure S2, Supporting Information, presents the results obtained after diluting the samples from Phantom Test 21 000 times and culturing them on three selective and differential media for 24 h. Figure 4c illustrates the microbial composition on the color-detection agar, corresponding to a 1000-fold dilution. The average cross-contamination levels for each sample corresponding to each channel are listed in Table 1. Samples collected from the last area yielded the lowest average cross-contamination rate of 0.2%. Examination of the

Table 1. Average cross-contamination percentage of each channel (n = 3).

Channel 1	Channel 2	Channel 3	Channel 4	Channel 5	Channel 6
0.4 ± 0.5%	$0.6 \pm 0.4\%$	$\textbf{0.4} \pm \textbf{0.5}\%$	$\textbf{0.8} \pm \textbf{0.4}\%$	$0.6\pm0.3\%$	$\textbf{0.2} \pm \textbf{0.3}\%$

cultivation results revealed slight microbial contamination in the test samples. However, the proportion of contaminated microbial colonies was 0.6 \pm 0.4% (n = 18), exerting minimal influence on the overall microbial composition. Consequently, through phantom tests, we verified that the proposed MSCR minimized cross-contamination and performed multi-sampling up to six times.

3.3. Ex Vivo Tests

Through ex vivo tests, we verified whether the proposed MSCR was capable of locomotion within actual organs, whether it could collect multiple microbiome samples from desired locations within an organ, and whether microbiome composition analysis was feasible through 16S rRNA sequencing analysis of the collected samples. **Figure 5**a and Video S4, Supporting Information,

26404567, 2025, 11, Downloaded from https://advanced.onlinelibrary.wiley.com/doi/10.1002/aisy.202300625 by Daegu Gyeongbuk Institute Of, Wiley Online Library on [27/11/2025]. See the Terms and Conditions (https://advanced.onlinelibrary.wiley.com/doi/10.1002/aisy.202300625 by Daegu Gyeongbuk Institute Of, Wiley Online Library on [27/11/2025]. See the Terms and Conditions (https://advanced.onlinelibrary.wiley.com/doi/10.1002/aisy.202300625 by Daegu Gyeongbuk Institute Of, Wiley Online Library on [27/11/2025]. See the Terms and Conditions (https://advanced.onlinelibrary.wiley.com/doi/10.1002/aisy.202300625 by Daegu Gyeongbuk Institute Of, Wiley Online Library on [27/11/2025]. See the Terms and Conditions (https://advanced.onlinelibrary.wiley.com/doi/10.1002/aisy.202300625 by Daegu Gyeongbuk Institute Of, Wiley Online Library on [27/11/2025]. See the Terms and Conditions (https://advanced.onlinelibrary.wiley.com/doi/10.1002/aisy.202300625 by Daegu Gyeongbuk Institute Of, Wiley Online Library.wiley.com/doi/10.1002/aisy.202300625 by Daegu Gyeongbuk Institute Of, Wiley Online Library.wiley.com/doi/10.1002/aisy.202300620 by Da

and-conditions) on Wiley Online Library for rules of use; OA articles are governed by the applicable Creative Commons License

www.advintellsvst.com

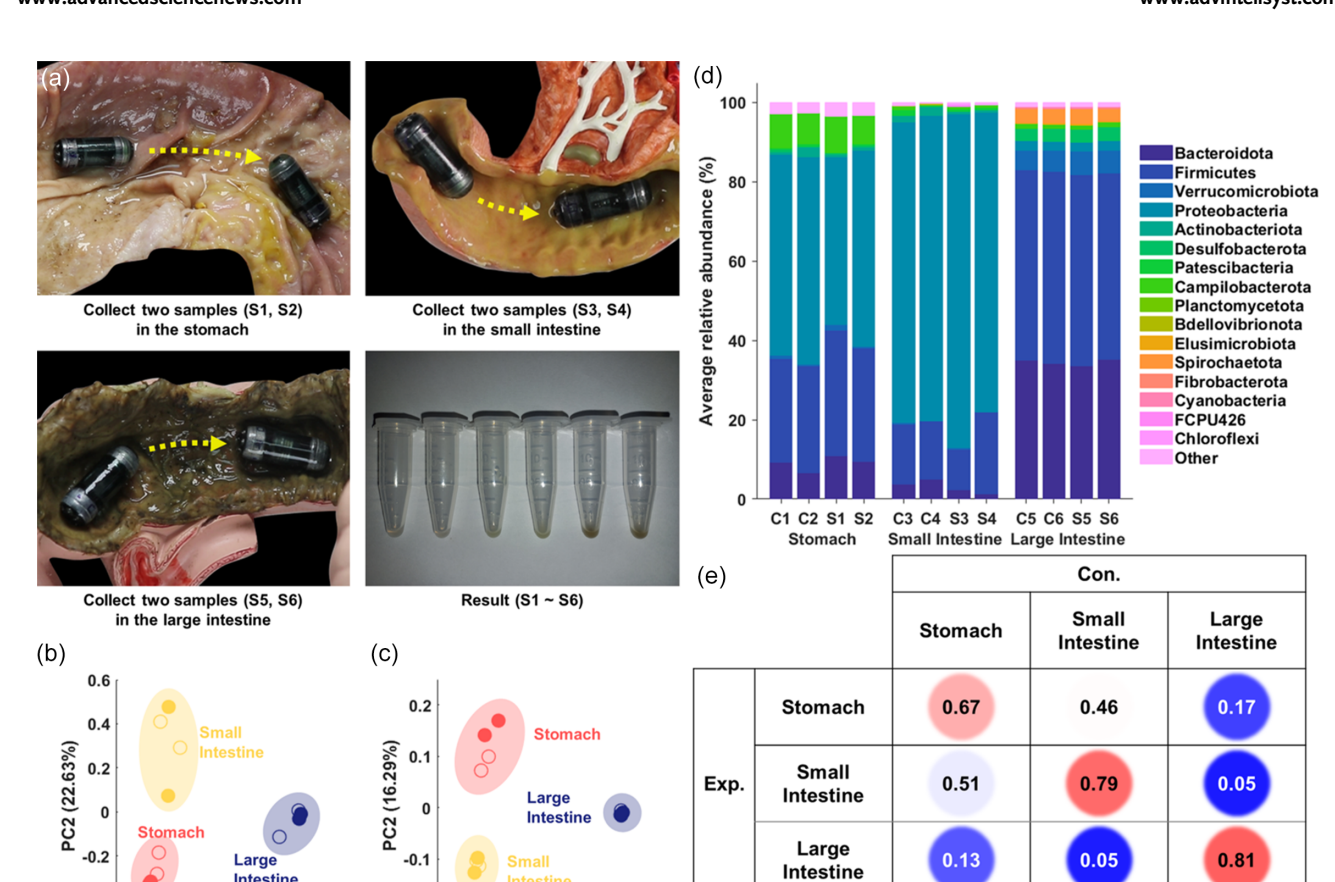


Figure 5. Ex-vivo tests results. a) Locomotion and multiple samplings of the capsule in each organ. b) Unweighted UniFrac PCoA results. c) Weighted UniFrac PCoA results. The unfilled symbols denote control samples extracted directly from each organ using a micropipette; the filled symbols denote experimental samples collected using the capsule. d) Relative abundance for different phyla in control samples (C1, C2, C3, C4, C5, and C6) and experimental samples (S1, S2, S3, S4, S5, and S6). e) Bray-Curtis similarity between the control samples and experimental samples.

show the process of collecting the microbial samples twice from each of the three organs using a single capsule, resulting in six samples. The average amount of the microbiome sample was \approx 9.9 \pm 1.7 mg (n = 6). On segments of the stomach, small intestine, and large intestine of a swine, fixed on a realistic GI model, the ability of the MSCR to locomote to target areas, perform two samplings at each location, and collect up to six microbiome samples in total was confirmed. Table S3 and S4, Supporting Information, present the unweighted and weighted UniFrac distance matrices, and Figure 5b,c show the principal coordinates analysis (PCoA) results calculated based on these distance matrices. The microbiome composition results of the control and experimental samples corresponding to each organ were consistent, which enabled the identification of three distinct clusters. Figure 5d shows the results of the relative abundance analysis wherein compositional differences were observed when comparing the microbiomes of the stomach, small intestine, and colon. Notably, analysis of control samples revealed that Proteobacteria and Firmicutes were the most abundant phyla in the stomach and small intestine, whereas Firmicutes and Bacteroidetes predominantly populated the colon. The stomach exhibited significantly higher levels of Campylobacterota than the small intestine.

Intestine

0 0.2

PC1 (26.25%)

-0.2

0

PC1 (79.84%)

0.2

-0.4

These key characteristics were consistently observed in the experimental samples collected using capsules. Figure 5e and S3-S5, Supporting Information, show the similarity in microbiome composition between the control and experimental samples. All four metrics confirmed that the microbiome composition of the directly collected samples was similar to that of the samples collected using the capsule.

3.4. In Vivo Tests

0.2

To verify the possibility of integration and the clinical applicability of the proposed MSCR, we conducted in vivo tests. Figure 6a shows a pig fixed on a bed with a movable external electromagnet system. Figure 6b shows the MSCR integrated with a camera module. Figure 6c and Video S5, Supporting Information, present the process of the MSCR moving within the stomach of the swine and collecting gastric fluids six times, as shown in the images captured by both the endoscope and camera module. Owing to the electromagnet of the movable external electromagnet system being positioned directly above the swine abdomen, the orientation and position of the capsule can be manipulated while in close contact with the upper wall of the stomach. As is

26404567, 2025, 11, Downloaded from https://ad-

onlinelibrary.wiley.com/doi/10.1002/aisy.202300625 by Daegu Gyeongbuk Institute Of, Wiley Online Library on [27/11/2025]. See the Terms

onditions) on Wiley Online Library for rules of use; OA articles are governed by the applicable Creative Commons License

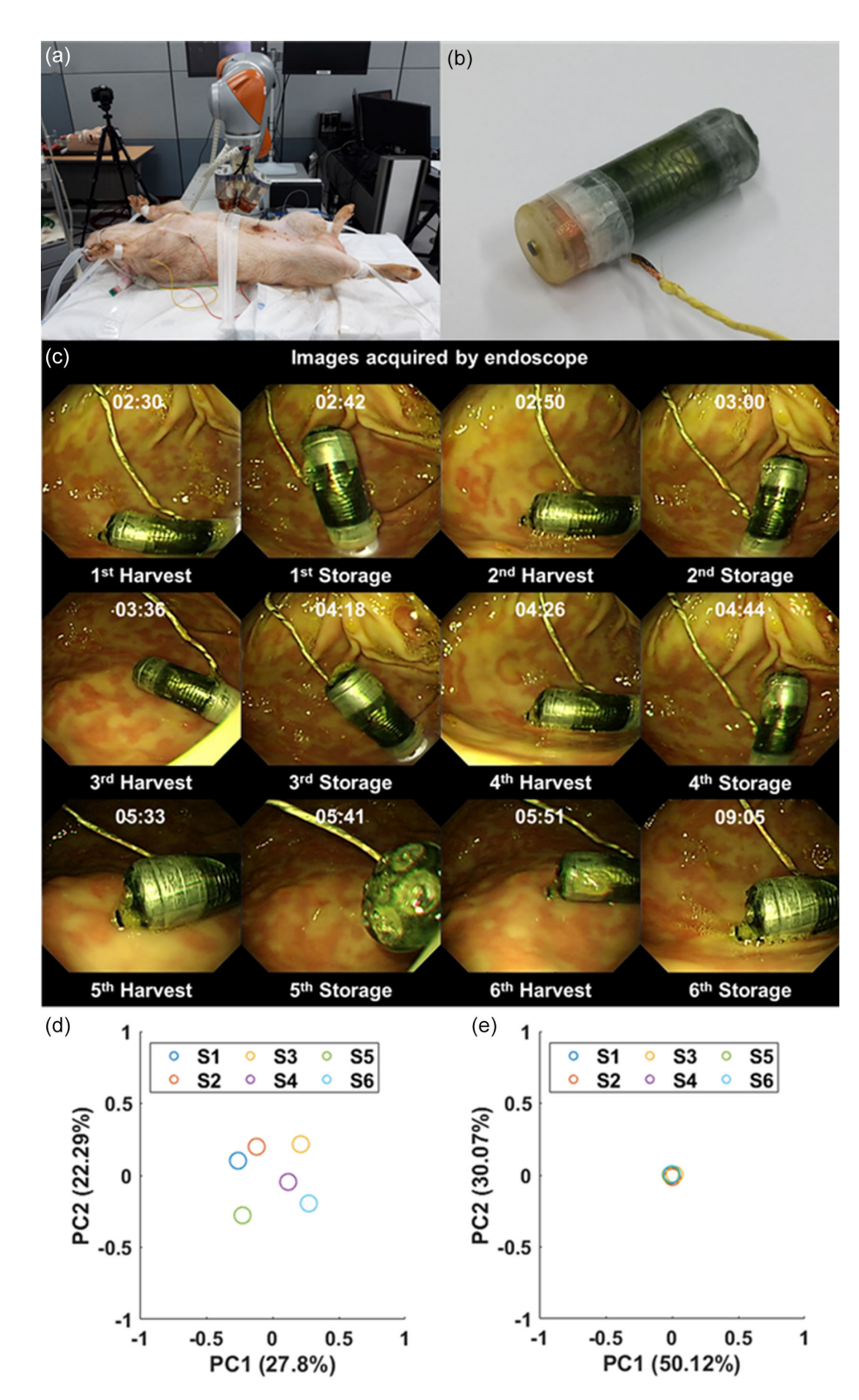


Figure 6. In-vivo tests results. a) Anesthetized swine and the movable external electromagnet system. b) MSCR integrated with a camera module. c) Locomotion and multiple samplings of the capsule in a porcine stomach. d) Unweighted UniFrac PCoA results. e) Weighted UniFrac PCoA results.



INTELLIGENT SYSTEMS

www.advancedsciencenews.com www.advintellsyst.com

evident from the images captured by the endoscope, the capsule actively controlled its posture and position within the stomach in an environment resembling clinical settings and successfully performed multisampling six times. Moreover, it was confirmed that the locomotion and intragastric microbial sampling of the proposed MSCR was feasible using a movable external electromagnet system rather than an electromagnetic coil system. Finally, we verified the real-time imaging capability of a living swine stomach using an additional camera module attached to the MSCR. Figure S6, Supporting Information, displays the cultivation responses of the Gifu anaerobic medium from the samples obtained during the in vivo experiments. Through additional cultures, we qualitatively confirmed the presence of the microbiome within the sample. Table S5 and S6, Supporting Information, present the unweighted/weighted UniFrac distance matrices, and Figure 6d,e show the unweighted/weighted UniFrac PCoA results derived from these matrices. The distances between the six samples were very small, revealing a single cluster and confirming high similarity among the six samples. Through this in vivo experiment, we verified that 16S rRNA sequencing analysis was possible using intragastric microbiome samples collected with MSCR.

3.5. Discussion

This study proposed the MSCR, which can collect up to six microbiome samples from the GI tract while minimizing cross-contamination. The locomotion and multiple-sampling performances of the MSCR were validated through various experiments. However, for the clinical application of MSCR, the following issues should be considered and addressed.

First, to obtain the gut microbiome from the desired location, it is necessary to recognize where the capsule reaches in the GI tract and whether the sampling tool contacts the intestinal wall. The MSCR used in this study was equipped with a wired camera module, which allowed the estimation of the sampling location through camera image, and microbiome sampling was performed accordingly. Here, the capsule motion could be influenced by the wire of the camera module. Therefore, a wireless camera module should be integrated into the MSCR. However, relying solely on an image from the wireless camera module to recognize the posture and location of MSCR within the GI tract has certain limitations. Consequently, there is a need to consider mounting a wireless localization module on the capsule or utilizing imaging systems like radiography and ultrasonography to accurately determine its posture and position within the GI tract.^[48,49]

Second, to achieve multiple samplings of the gut microbiome, the proposed MSCR operated by employing grooves on the inner side of the capsule body, upward and downward movements of the driving unit, and deployment and storage of the sampling tool. During this multiple-sampling process of the MSCR, if a significant external force acted on the capsule, certain issues may be encountered, such as the sampling tool dropping from the channel or not sequentially deploying one at a time. Furthermore, the MSCR does not provide a method for confirming whether the sampling tool has been successfully deployed or stored during the sampling process. Fundamental experiments

confirmed the successful and consistent operation of the multiple-sampling mechanism by deploying and storing the sampling tool 100 times for each channel. However, these validations were conducted under ideal conditions, where the external force exerted on the capsule was not significant and the capsule posture remained unchanged. Therefore, to ensure reliable operation of the MSCR, precision must be ensured during the manufacturing process of each capsule component and improvements toward the mechanism should be considered such that it is structurally robust to external forces.

Third, the microbiome composition of the collected sample can change from the time of sampling using MSCR until its retrieval. The microbiome composition of a sample can be changed by the metabolic activity of the microbiome and the death of the anaerobic microbiome due to oxygen exposure. The analysis of a sample with a distorted microbiome composition results in misunderstandings regarding the functions and roles of gut microbes. In this study, the samples retrieved from the MSCR were immediately stored in a frozen state to stabilize the microbiome composition. However, the effectiveness of this method has not yet been rigorously addressed. Consequently, reagents must be incorporated into the sampling tool to inhibit microbial metabolic activity or to develop a post-processing protocol for the samples considering the oxygen concentration after the retrieval of the MSCR.^[50–52]

4. Conclusion

This study proposes an MSCR capable of collecting microbiome samples from various locations within the GI tract while minimizing cross-contamination. The proposed capsule comprised a capsule body with six channels, an inner groove, a driving unit powered by magnetic fields and responsible for the operation of six sampling tools that can seal the channel entrances before and after sample collection, a central rod designed to guide the movement of the driving unit along the central axis, and two capsule heads positioned at the top and bottom. The capsule is controllable using external magnetic fields, enabling adjustments in its posture, position, and alignment with the desired channel toward the intestinal surface. In addition, the capsule was equipped with a multiple-sampling mechanism and a cross-contamination prevention structure, facilitating the collection of up to six microbiome samples, while preventing contamination before and after each collection. Through basic performance tests, we implemented and evaluated the capsule propulsion, channel alignment, and sample collection and storage capabilities of the MSCR (propulsion direction precision: $0.76 \pm 0.52^{\circ}$, channel alignment precision: $0.84 \pm 0.55^{\circ}$). We evaluated the active locomotion and multiple-sampling performance of the MSCR through the phantom tests (average amount per sample: $10.3 \pm 2.4 \, \text{mg}$ from 18 samples, cross-contamination: $0.6 \pm 0.4\%$) and exvivo tests (average amount per sample: 9.9 ± 1.7 mg from 6 samples) in an environment simulating the human intestine. Furthermore, the microbiome composition of the samples was analyzed both qualitatively and quantitatively. Subsequent in vivo tests verified that the camera module could be mounted on the MSCR, and its active locomotion and multiple sampling were confirmed within a porcine stomach environment. Future enhancements to MSCR

ADVANCED SCIENCE NEWS

ADVANCED INTELLIGENT SYSTEMS

www.advancedsciencenews.com www.advintellsyst.com

are anticipated through miniaturization of the capsule, integration of the wireless localization module, and the development of protocols for sample storage and retrieval. In conclusion, MSCR is expected to play a pivotal role in the near future by tracking spatiotemporal changes in the gut microbiome within the human body, thereby contributing to a deeper understanding of GI diseases and the development of personalized diagnostic and therapeutic approaches.

5. Experimental Section

Fabrication of MSCR: The proposed MSCR was fabricated using the following procedure. First, the capsule body, central rod, upper head, and lower head were produced using stereolithography (SLA) 3D printing (SLA 600, ProtoFab) with an acrylonitrile butadiene styrene (ABS)-like transparent resin material (Clara A, ProtoFab). The printed components were coated with polyaniline (PANI) to obtain a hydrophilic surface. [53] The solution used for PANI coating was prepared by adding aniline monomer (10 mM) and ammonium persulfate (6.7 mM) to perchloric acid (1 M, 100 mL) (Sigma Aldrich, USA). The fabricated parts were immersed in the mixture solution, stirred for $\approx\!24\,\text{h}$ at 4 °C, and then rinsed with DI water. The resulting components were highly transparent, precise, super hydrophilic, and biocompatible. [54]

Second, the driving unit was fabricated as follows. Initially, to assemble the permanent magnet assembly, five axially magnetized ring permanent magnets (ARPMs) with an outer diameter, outer diameter, and height of 8.0, 2.3, and 1 mm, respectively were used along with a radially magnetized ring permanent magnet (RRPM) of the same size. The permanent magnet assembly was created by sequentially placing two ARPMs, one RRPM, and three ARPMs inside a hollow cylinder and solidifying them with epoxy (Gorilla epoxy and glue). The theoretical magnetization angle (θ_T) of the fabricated permanent magnet assembly was calculated using a simple vector sum as 11.1°. The measured magnetization angle ($\theta_{\rm M}$) of the permanent magnet assembly was ≈11.1°, confirming its consistency with the theoretically calculated angle. Furthermore, a soft magnetic rod made of SUS440C material (MRSS1.0-5.5-AC0.5, Misumi) and two hemispherical pins (YAAA) in the driving unit were affixed to the top and side surfaces, respectively, considering the magnetization direction of the permanent magnet assembly using a UV-curable adhesive (LOCTITE 4306, Henkel).

Third, the sampling tool comprised nitrile rubber, iron rubber, supports, and a brush. The sampling tool was fabricated using the following process. First, a nitrile rubber sheet with a thickness of 0.5 mm (RBNM0.5-500, Misumi) was punched using a 2.5 mm diameter hole punch tool to produce the nitrile rubber component. Similarly, an iron rubber sheet with a thickness of 0.5 mm (JLS-M5040, Misumi) was punched using a 2.0 mm diameter hole punch tool to produce the iron rubber component. The magnetic characteristics of the iron rubber are shown in Figure S1, Supporting Information. Next, the first and second supports, matching the diameters and heights of the nitrile and iron rubber, respectively, were fabricated using an SLA 3D printer (Form 3, Formlabs) with a semi-transparent resin (clear resin, Formlabs). The brush was created by cutting a 2.0 mm diameter brush (brush4u) to a length of 5.0 mm. Finally, the first support, nitrile rubber, brush, second support, and iron rubber were sequentially placed inside a hollow cylinder and solidified using an adhesive to fabricate the sampling tool.

Experimental Setup 1 (Electromagnetic Coil System): An electromagnetic coil system was designed to validate the basic performance of the MSCR. As shown in Figure 2a, the electromagnetic coil system comprised three-axis Helmholtz coils, a camera, and a 3D-printed jig. The specifications of the three-axis Helmholtz coils are listed in Table S1, Supporting Information. During the motion-control process of the MSCR, a magnetic field was generated using all three axes of the Helmholtz coils, whereas a magnetic field gradient was produced using only the z-axis Helmholtz coil. A conventional joystick was employed to facilitate motion control of the MSCR. The magnetic fields and forces applied in real-time to the MSCR

and the corresponding currents applied to the electromagnetic coil system were calculated in a LabVIEW environment. The computed currents were then applied to the three Helmholtz coils using a compact DAQ (cDAQ-9174, National Instruments) and a motion controller (B30A40AC, Advanced Motion Controls). The maximum current was limited to 20 A to ensure the safe operation of the EMA system. The maximum intensity of the magnetic field was $\approx\!65$ mT, and that of the magnetic field gradient was $\approx\!137$ mT m $^{-1}$. A 3D-printed jig was employed to confine the movement of the proposed MSCR within the ROI. Finally, the experimental process and results were recorded using a DSLR camera (EOS-800D, CANON).

Experimental Setup 2 (Movable External Electromagnet System): A movable external electromagnet system was designed to verify the clinical applicability of the MSCR. As depicted in Figure 2b, the movable external electromagnet system comprised a 7 degree-of-freedom robotic arm (LBR iiwa 7 R800, KUKA) and a hybrid magnetic actuator. The hybrid magnetic actuator comprising two hybrid magnets combined at 30° can generate both static and dynamic magnetic fields. Each hybrid magnet was composed of a cylindrical neodymium magnet (diameter: 70 mm, length: 60 mm), a solenoid coil (using a 1.5 mm diameter electric wire, with 304 turns), and a soft magnetic core (Vacoflux, diameter: 22 mm, length: 125 mm). The static magnetic field, which used only the robotic arm, facilitated capsule movement along the x-, y-, and z-axes and performed the yaw motion. The dynamic magnetic field can change the direction of the static magnetic field over time, enabling the pitch motion of the capsule. Therefore, the four basic movements of the MSCR can be executed using a hybrid magnetic actuator and robotic arm. In actual applications, a static magnetic field is first applied while simultaneously manipulating the robotic arm to move the capsule to the desired position. Subsequently, a dynamic magnetic field was applied to momentarily align the capsule posture upright, allowing the driving unit inside to move, execute deployment, and store the sampling tool. Using a movable external electromagnet system, MSCR can perform 5 degree-of-freedom movements and multiple samplings within the GI tract. In the proposed magnetic actuator structure, a maximum current of 20 A applied to the electromagnet generated the maximum magnetic field of ≈100 mT and the magnetic field gradient of $\approx 3 \,\mathrm{T\,m}^{-1}$. In addition, considering the allowable distance of the utilized 7 degree-of-freedom robotic arm, the capsule could operate within length, width, and height ranges of 800, 500, and 300 mm, respectively.

Basic Performance Tests: Three experiments were conducted using an MSCR and an electromagnetic coil system to evaluate its fundamental performance. First, an experiment was conducted to align and propel the capsule in the desired direction. The capsule was placed in a jig containing a PEG 10 000 solution with a viscosity similar to that of intestinal fluid. Here, the viscosity of the PEG 10 000 solution was measured to be 100 mPa s⁻¹ (4 °C, 101.3 kPa) using a rotary viscous meter (SNB-2), and the jig used in the experiment was fabricated using a 3D printer (DP200, Sindoh). The propulsion direction was set in eight directions ranging as 0°-360° at intervals of 45°. A magnetic field was applied to align the capsule in each direction, followed by a magnetic field gradient to propel it. Image analysis was used to measure the angle of the propulsion direction of the capsule, and the difference between the set and measured propulsion direction angles was derived. Subsequently, an experiment was conducted to rotate the capsule in the roll direction to align the desired channel toward the bottom surface. A magnetic field was applied using a sampling tool deployed to align the channels and the bottom surface of the capsule was photographed. The captured images were analyzed to measure the roll angle of the capsule and the channel alignment angle error was determined. Third, an experiment was conducted to deploy and store the six sampling tools inside the capsule. To measure the probability of failure in deployment and storage, both processes were repeated 100 times, six times each, and the results were photographed each time a sampling tool was deployed or stored.

Phantom Tests: To validate the locomotion and multiple-sampling capabilities of the MSCR, two phantom tests were conducted using the MSCR and an electromagnetic coil system. A model with an intestinal shape, including five well-like regions, was fabricated using a 3D printer

ADVANCED SCIENCE NEWS ADVANCED Intelligent Systems

www.advancedsciencenews.com www.advintellsyst.com

(DP200, Sindoh). To mimic the human small intestine, fresh porcine intestines were adhered to the walls of the model using adhesives to complete the phantom. Target solutions of ≈ 3 mL were injected into the first, third, and fifth regions of the phantom, and buffer solutions of ≈ 3 mL were injected into the second and fourth regions of the phantom. Saline was used as a buffer to dilute or wash away any solution adhering to the exterior of the capsule. This was performed to reduce contamination from the previous target solution in the subsequent target regions. To match the viscosity of the intestinal fluid, PEG 10 000 (Sigma-Aldrich) was added to both the target and buffer solutions at a ratio of 30% w/v.

In Phantom Test 1, three different colored saline solutions (0.85%) were used as the target solutions to visually examine the degree of contamination. Yellow, red, and blue solutions were placed in the first, third, and fifth regions of the phantom, respectively. Using the MSCR, sampling from each target region was conducted twice, resulting in six samples from three target regions using the proposed capsule. Subsequently, the samples stored in each channel of the proposed capsule were carefully extracted using a micropipette.

In Phantom Test 2, three different types of microbial culture solutions were employed as target solutions to qualitatively and quantitatively analyze the degree of sample contamination. The microbes used in this experiment are commonly found in the human digestive system and can be easily cultivated. The following three microbes were selected from the Korea Culture Center of Microorganisms: Enterococcus faecalis (ATCC 29 212), Escherichia coli (ATCC 10 798), and Proteus mirabilis (ATCC 21 100). The selected microbes were cultured in tryptone Agar/Broth supplemented with NaCl, nutrient Agar/Broth, and trypticase soy Agar/Broth supplemented with defibrinated sheep blood (Difco). Cultures of E. faecalis, E. coli, and P. mirabilis were placed in the first, third, and fifth regions, respectively. Six microbial samples were obtained using the MSCR, consistent with Phantom Test 1. To evaluate the sampled microbes, three types of selective and differential media were used: MacConkey Agar (Difco), Bile Esculin Agar (Difco), and color-detection agar (MB Cell). The expected culture reactions for each medium are summarized in Table S2, Supporting Information. Each sample was diluted in saline to a decimal dilution range of 10^{-3} – 10^{-5} , inoculated onto each selective and differential medium, and subsequently incubated at 37 °C for 24 h. The microbial counts in the target solutions were determined using an aerobic count plate (3 M). The microbial counts in the target solutions were 1.4×10^7 , 5.0×10^7 , and 1.4×10^7 CFU mL⁻¹ for E. faecalis, E. coli, and P. mirabilis, respectively.

Ex Vivo Tests: Ex vivo tests were conducted using the proposed MSCR and an electromagnetic coil system. This experiment aimed to verify the feasibility of capsule locomotion and multiple sampling in an ex vivo environment using MSCR, and the possibility of conducting 16S rRNA sequencing analysis with the obtained samples. Finally, a comparative analysis was conducted between the microbiome composition of samples directly extracted from the intestines (control group) and those acquired via the proposed MSCR (experimental group). Freshly slaughtered porcine stomach, small intestine, and large intestine segments were fixed to corresponding realistic GI models. Initially, two samples were collected from three organs using a micropipette, yielding six control samples. Subsequently, a single MSCR was used to move the capsule to the target areas within each organ segment, followed by two samplings. The samples stored in the MSCR channels were carefully retrieved using a micropipette, resulting in six experimental group samples. Each sample was mixed with $40\,\mu L$ of sterile saline and $50\,\mu L$ of a 50% v/v glycerol solution. Subsequently, they were immediately frozen and stored in a -80 °C deep freezer. All samples were subjected to 16S rRNA sequencing. The amplicon sequence variant (ASV) data were used to determine relative abundance within the samples. The microbiome compositional similarity between the samples was calculated using UniFrac weighted/unweighted metrics. The derived similarity matrix was visualized using PCoA. Finally, the average microbiome compositions of the control and experimental group samples were determined for each organ, and microbiome compositional similarities were analyzed for the six datasets.

In- Vivo Tests: The clinical applicability of MSCR was assessed by verifying its locomotion and multiple-sampling performance within the

stomachs of live swine. In the experiment, the MSCR was integrated with a camera module (AMC-6946, DOTHECAMERA). The orientation and position of the MSCR within the stomach were controlled using a movable external electromagnetic system. In contrast to an electromagnetic coil system, a movable external electromagnet system can generate a stronger magnetic force, has a relatively large ROI, and is more suitable for clinical applications. The in-vivo testing procedure commenced with the secure placement of an anesthetized pig on a medical bed. Subsequently, an overtube, designed for the administration of the capsule was inserted into the esophagus of the pig. The prepared capsule was then introduced through the overtube and guided into the stomach using an endoscope (Q160AL, Olympus). The entire procedure was recorded using the endoscope and the camera module integrated into the MSCR (OV6946, dothecamera). After completing the experiment, the endoscope, equipped with a snare, was utilized to retrieve the capsule from the stomach. Each sample was mixed with 40 μ L of sterile saline and 50 μ L of a 50% v/v glycerol solution, and then stored in a deep freezer. To verify the presence of microbes in the samples, each sample was inoculated onto a medium and incubated at 37 °C for 24 h in a microaerophilic environment. Gifu anaerobic medium (mb cell), anaeropack (MGC), and a 2.5 L rectangular jar were used for sample cultivation. In addition, 16S rRNA sequencing was performed on the samples. The microbiome compositional similarity between the samples was examined using the obtained ASV data.

Supporting Information

Supporting Information is available from the Wiley Online Library or from the author

Acknowledgements

This work was supported by the National Research Foundation (NRF), founded by the Ministry of Science and ICT (NRF-2021R1A2C3007817), the DGIST R&D Program of the Ministry of Science and ICT (23-PCOE-02), and the Korea Health Technology Development R&D Project through the Korea Health Industry Development Institute (KHIDI), funded by the Ministry of Health & Welfare (RS-2023-00302150), Republic of Korea.

Conflict of Interest

The authors declare no conflict of interest.

Data Availability Statement

The data that support the findings of this study are available from the corresponding author upon reasonable request.

Keywords

capsule endoscopy, electromagnetic actuation (EMA), gastrointestinal (GI) tract, gut microbiota, multiple-sampling capsule robot, multipoint sampling

Received: October 1, 2023 Revised: April 8, 2024 Published online: June 3, 2024

[1] M. Afzaal, F. Saeed, Y. A. Shah, M. Hussain, R. Rabail, C. T. Socol, A. Hassoun, M. Pateiro, J. M. Lorenzo, A. V. Rusu, R. M. Aadil, Front. Microbiol. 2022, 13, 999001.

www.advancedsciencenews.com www.advintellsyst.com

- [2] J. M. Pickard, M. Y. Zeng, R. Caruso, G. Núñez, Immunol. Rev. 2017, 279. 70.
- [3] Z. Y. Kho, S. K. Lal, Front. Microbiol. 2018, 9, 356589.
- [4] I. Rowland, G. Gibson, A. Heinken, K. Scott, J. Swann, I. Thiele, K. Tuohy, Eur. J. Nutr. 2018, 57, 1.
- [5] I. Khan, N. Ullah, L. Zha, Y. Bai, A. Khan, T. Zhao, T. Che, C. Zhang, Pathogens 2019, 8, 126.
- [6] R. Pittayanon, J. T. Lau, G. I. Leontiadis, F. Tse, Y. Yuan, M. Surette, P. Moayyedi, Gastroenterology 2020, 158, 930.
- [7] A. Lavelle, H. Sokol, Nat. Rev. Gastroenterol, Hepatol. 2020, 17, 223.
- [8] L. Crovesy, D. Masterson, E. L. Rosado, Eur. J. Clin. Nutr. 2020, 74. 1251.
- [9] M. Duan, Y. Wang, Q. Zhang, R. Zou, M. Guo, H. Zheng, PLoS One **2021**, 16, 0255446.
- [10] M. Gurung, Z. Li, H. You, R. Rodrigues, D. B. Jump, A. Morgun, N. Shulzhenko, EBioMedicine 2020, 51.
- [11] H. Wu, V. Tremaroli, C. Schmidt, A. Lundqvist, L. M. Olsson, M. Krämer, A. Gummesson, R. Perkins, G. Bergström, F. Bäckhed, Cell Metab. 2020, 32, 379.
- [12] Y. Jiao, L. Wu, N. D. Huntington, X. Zhang, Front. Immunol. 2020, 11, 503395
- [13] H. Xu, M. Liu, J. Cao, X. Li, D. Fan, Y. Xia, X. Lu, J. Li, D. Ju, H. Zhao, J. Immunol. Res. 2019, 2019.
- [14] W. Fong, Q. Li, J. Yu, Oncogene 2020, 39, 4925.
- [15] S. H. Wong, J. Yu, Nat. Rev. Gastroenterol. Hepatol. 2019, 16, 690.
- [16] Z. Amirkhanzadeh Barandouzi, A. R. Starkweather, W. A. Henderson, A. Gyamfi, X. S. Cong, Front. Psychiatry 2020, 11, 1.
- [17] T. T. Huang, J. B. Lai, Y. L. Du, Y. Xu, L. M. Ruan, S. H. Hu, Front. Genet. 2019, 10, 435190.
- [18] C. A. Simpson, C. Diaz-Arteche, D. Eliby, O. S. Schwartz, J. G. Simmons, C. S. M. Cowan, Clin. Psychol. Rev. 2021, 83, 101943.
- [19] M. Xu, X. Xu, J. Li, F. Li, Front. Psychiatry 2019, 10, 473.
- [20] S. Wu, X. Liu, R. Jiang, X. Yan, Z. Ling, Front. Aging Neurosci. 2021, 13, 650047.
- [21] A. Beam, E. Clinger, L. Hao, Nutrients 2021, 13, 2795.
- [22] E. R. Leeming, A. J. Johnson, T. D. Spector, C. I. L. Roy, Nutrients 2019 11 1
- [23] C. Mu, W. Zhu, Appl. Microbiol. Biotechnol. 2019, 103, 9277.
- [24] J. Aragón-Vela, P. Solis-Urra, F. J. Ruiz-Ojeda, A. I. Álvarez-Mercado, J. Olivares-Arancibia, J. Plaza-Diaz, Nutrients 2021, 13, 3999.
- [25] A. Lavelle, G. Lennon, O. O'Sullivan, N. Docherty, A. Balfe, A. Maguire, H. E. Mulcahy, G. Doherty, D. O'Donoghue, J. Hyland, R. P. Ross, J. C. Coffey, K. Sheahan, P. D. Cotter, F. Shanahan, D. C. Winter, P. R. O'Connell, Gut 2015, 64, 1553.
- [26] J. U. Dahl, M. J. Gray, D. Bazopoulou, F. Beaufay, J. Lempart, M. J. Koenigsknecht, Y. Wang, J. R. Baker, W. L. Hasler, V. B. Young, D. Sun, Nat. Microbiol. 2017, 2, 1.
- [27] R. B. Sartor, Nat. Rev. Gastroenterol. Hepatol. 2015, 12, 253.
- [28] F. E. R. Vuik, J. Dicksved, S. Y. Lam, G. M. Fuhler, L. J. W. van der Laan, A. van de Winkel, S. R. Konstantinov, M. C. W. Spaander, M. P. Peppelenbosch, L. Engstrand, E. J. Kuipers, United Eur. Gastroenterol. J. 2019, 7, 897.
- [29] N. Zmora, G. Zilberman-Schapira, J. Suez, U. Mor, M. Dori-Bachash, S. Bashiardes, E. Kotler, M. Zur, D. Regev-Lehavi, R. B. Z. Brik, S. Federici, Cell 2018, 174, 1388.
- [30] A. M. Seekatz, M. K. Schnizlein, M. J. Koenigsknecht, J. R. Baker, W. L. Hasler, B. E. Bleske, V. B. Young, D. Sun, mSphere 2019, 4, 10.

- [31] G. G. S. Leite, S. Weitsman, G. Parodi, S. Celly, R. Sedighi, M. Sanchez, W. Morales, M. J. Villanueva-Millan, G. M. Barlow, R. Mathur, S. K. Lo, Dig. Dis. Sci. 2020, 65, 2595.
- [32] E. R. Shanahan, L. Zhong, N. J. Talley, M. Morrison, G. Holtmann, Aliment. Pharmacol. Ther. 2016, 44, 648.
- [33] S. M. Huse, V. B. Young, H. G. Morrison, D. A. Antonopoulos, J. Kwon, S. Dalal, R. Arrieta, N. A. Hubert, L. Shen, J. H. Vineis, I. C. Koval, Microbiome 2014, 2, 1.
- [34] A. Lavelle, G. Lennon, N. Docherty, A. Balfe, H. E. Mulcahy, G. Doherty, D. O'Donoghue, J. M. Hyland, F. Shanahan, K. Sheahan, J. C. Coffey, PLoS One 2013, 8, e78835.
- [35] G. B. Saffouri, R. R. Shields-Cutler, J. Chen, Y. Yang, H. R. Lekatz, V. L. Hale, J. M. Cho, E. J. Battaglioli, Y. Bhattarai, K. J. Thompson, K. K. Kalari, Nat. Commun. 2019, 10, 2012.
- [36] D. O. Otuya, Y. Verma, H. Farrokhi, L. Higgins, M. Rosenberg, C. Damman, G. J. Tearney, Expert Rev. Gastroenterol. Hepatol. 2018, 12, 109.
- [37] Q. Tang, G. Jin, G. Wang, T. Liu, X. Liu, B. Wang, H. Cao, Front. Cell. Infect. Microbiol. 2020, 10, 151.
- [38] D. Shalon, R. N. Culver, J. A. Grembi, J. Folz, P. V. Treit, H. Shi, F. A. Rosenberger, L. Dethlefsen, X. Meng, E. Yaffe, A. Aranda-Díaz, Nature 2023, 617, 581.
- [39] S. Nejati, J. Wang, S. Sedaghat, N. K. Balog, A. M. Long, U. H. Rivera, V. Kasi, K. Park, J. S. Johnson, M. S. Verma, R. Rahimi, Acta Biomater. 2022, 154, 83,
- [40] H. Rezaei Nejad, B. C. M. Oliveira, A. Sadeqi, A. Dehkharghani, I. Kondova, J. A. M. Langermans, J. S. Guasto, S. Tzipori, G. Widmer, S. R. Sonkusale, Adv. Intell. Syst. 2019, 1, 1900053.
- [41] F. Soto, E. Purcell, M. O. Ozen, P. D. Sinawang, J. Wang, D. Akin, U. Demirci, Adv. Intell. Syst. 2022, 4, 2200030.
- [42] M. Rehan, I. Al-Bahadly, D. G. Thomas, E. Avci, IEEE Rob. Autom. Lett. 2022, 7, 9517.
- [43] P. Shokrollahi, Y. P. Lai, S. Rash-Ahmadi, V. Stewart, M. Mohammadigheisar, L. A. Huber, N. Matsuura, A. E. H. Zavodni, J. Parkinson, E. Diller, IEEE/ASME Trans. Mechatron. 2020, 26, 2616.
- [44] D. Ye, J. Xue, S. Yuan, F. Zhang, S. Song, J. Wang, M. Q. H. Meng, IEEE Trans. Biomed. Eng. 2022, 69, 2905.
- [45] C. Lee, H. Choi, G. Go, S. Jeong, S. Y. Ko, J. O. Park, S. Park, IEEE/ ASME Trans. Mechatron. 2015, 20, 2067.
- [46] M. C. Hoang, K. T. Nguyen, V. H. Le, J. Kim, E. Choi, J. Park, C. Kim, IEEE Trans. Syst. Man Cybern. Syst. 2019, 51, 3040.
- [47] S. Park, H. Lee, D. I. Kim, H. Kee, S. Park, IEEE/ASME Trans. Mechatron. 2022, 27, 4384.
- [48] S. L. Liu, J. Kim, B. Kang, E. Choi, A. Hong, J. O. Park, C. S. Kim, IEEE Access 2020, 8, 141159.
- [49] S. L. Liu, J. Kim, A. Hong, J. O. Park, C. S. Kim, IEEE Access 2022, 10, 22865.
- [50] S. Bellali, J. C. Lagier, D. Raoult, J. B. Khalil, Front. Microbiol. 2019, 10,
- [51] N. Martínez, C. Hidalgo-Cantabrana, S. Delgado, A. Margolles, B. Sánchez, Sci. Rep. 2019, 9, 8327.
- [52] M. Rios-Morales, M. P. H. van Trijp, C. Rösch, R. An, T. Boer, A. Gerding, N. de Ruiter, M. Koehorst, M. R. Heiner-Fokkema, H. A. Schols, D. J. Reijngoud, Sci. Rep. 2021, 11, 8133.
- [53] N. R. Chiou, C. Lu, J. Guan, L. J. Lee, A. J. Epstein, Nat. Nanotechnol.
- [54] P. Humpolicek, V. Kasparkova, P. Saha, J. Stejskal, Synth. Met. 2012, 162, 722.